Solid State Sciences 51 (2016) 51–58

Contents lists available at ScienceDirect

Solid State Sciences

journal homepage: www.elsevier.com/locate/ssscie

Preparation and characterization of platinum (Pt) and palladium (Pd) nanoparticle decorated graphene sheets and their utilization for the elimination of basic fuchsin and indigo carmine dyes

Belma Zengin Kurt [a], Zehra Durmus [b, *], Ali Durmus [c]

[a] Department of Pharmaceutical Chemistry, Faculty of Pharmacy, Bezmialem Vakif University, Fatih, 34093 Istanbul, Turkey
[b] Department of Pharmaceutical Biotechnology, Faculty of Pharmacy, Bezmialem Vakif University, Fatih, 34093 Istanbul, Turkey
[c] Department of Chemical Engineering, Faculty of Engineering, Istanbul University, Avcılar, 34320 Istanbul, Turkey

ARTICLE INFO

Article history:
Received 2 November 2015
Received in revised form
22 November 2015
Accepted 23 November 2015
Available online 2 December 2015

Keywords:
Graphene
Noble metal nanoparticle
Nanocomposite
Antioxidant activity
Photocatalytic degradation

ABSTRACT

In this study, graphene nano sheets, prepared with chemical oxidation and reduction routes via modified-Hummer method, were successfully decorated with platinum (Pt) and palladium (Pd) nanoparticles. Structural and morphological features of resulted graphene-metal nanocomposites were characterized with FT-IR, XRD, SEM and TEM methods. Anti-oxidant activity (AOA) values of nanocomposites were determined. The IC_{50} values of Pt-graphene and Pd-graphene nanocomposites were found to be 46.1 and 90.2 μg/mL, respectively based on the ABTS method and 80.2 and 143.7 μg/mL according to the DPPH method. It was found that the graphene-metal nanocomposites exhibited superior free radical scavenging activity compared to several types of noble metal nano particles although the nanocomposites consist of much lower amount of active metal sites than the nano-crystalline metal powders. It was consequently reported that the graphene-metal nanocomposites could be successfully used for the photocatalytic elimination of fuchsin and indigo carmine dyes under light irradiation.
© 2015 Elsevier Masson SAS. All rights reserved.

1. Introduction

Graphene, known as the “thinnest material in our universe” and a one-atom-thick layer of hexagonally arrayed sp^2-bonded carbon atoms tightly packed into a two-dimensional (2D) crystal of hybridized carbon with honeycomb lattice, is one of the unique carbon structures having some physical and geometrical features [1]. Graphene can also be defined as the basal building block in all graphitic materials [2]. Considering of its structural and geometrical properties such as large surface area (theoretically 2630 m^2/g, [3]), high carrier concentration and mobility, excellent electrical conductivity and high modulus, graphene has attracted a great research attention, in the both theoretical and experimental points of view, in various applications in the materials science and engineering, in recent years. Unfortunately, technological applications of graphene are still quite limited because the preparation of a graphene layer or a few-atom-thick stacks consisting of several layers requires difficult and expensive chemical and/or physical processes and also due to the lack of mass-production processes for graphene, yet. The most widely used practical methods for the preparation of graphene nano sheets are chemical oxidation and reduction of graphite and thermal expansion of oxidized graphite in high temperatures.

The preparation and characterization of nano structured metal particles is another widely studied research subject in materials science in a last few decades due to a wide application potential and technical advantages of such materials by considering of their physicochemical properties such as stability, conductivity, biocompatibility, and low cytotoxicity [4]. Large surface area and manipulation of physicochemical properties of graphene surfaces via several physical and/or chemical modification routes such as irradiation with plasma atmosphere, chemical oxidation, grafting with organic groups etc. make the 2D graphene very attractive and convenient template for uniform deposition and formation of metal nanoparticles and also laterally dispersion because the graphene layers may induce and prevent the agglomeration of nanoparticles.

Synthesis of metal nanoparticles onto different types of carbon materials and the utilization of resulted carbon-metal nanocomposites in different applications have been studied [5–11]. It is a well-known fact that the noble metal nanoparticles, e.g. platinum

* Corresponding author.
E-mail address: zdurmus@bezmialem.edu.tr (Z. Durmus).

http://dx.doi.org/10.1016/j.solidstatesciences.2015.11.012
1293-2558/© 2015 Elsevier Masson SAS. All rights reserved.

(Pt), palladium (Pd) and, gold (Au) nanoparticles are highly effective catalysts, in several reactions such as hydration, hydrogenation, and oxidation due to their relatively large surface area and the high proportion of metal atoms located on their surfaces [12]. These metal nanoparticles can be considered as potentially useful materials in medical science and clinical therapy as they also act as antioxidants [13]. Some studies on the strong antioxidant activity of Pt nanoparticles have been reported [14–17]. Preparation of noble metal nanoparticles onto various types of carbon nano materials have also been reported. Do and Drzal synthesized Pt nanoparticles on different carbon nanostructures, namely single and multiwalled carbon nanotube (SWNT and MWCNT), carbon black (CB), and graphite nanofiber (GNF), in the absence and presence of various room temperature ionic liquids (RTILs) by a microwave process and investigated [18]. They reported that the RTIL-assisted microwave process yielded metal nanoparticles with an average particle size of 2 nm and having a narrow size distribution due to the function of RTIL acting as a promoting agent to increase the reduction rate of a metal salt, a protecting agent to prevent metal particles from growing and agglomerating each other. Garrido et al. prepared silver (Ag) and Pd decorated carbon nanotube composites via super critical fluid assisted method as a simple, rapid and green procedure [19]. They concluded that the supercritical fluids assisted chemical deposition method appeared as an interesting alternative process for the uniform decoration of CNTs with strong interfaces for the preparation of composite materials. Zheng et al. prepared a series of graphene oxide (GO)/noble metal (Au, Pt, and Pd) nanoparticle composites via a one-step hydrothermal method [20]. They showed that the metal nanoparticles with different average sizes and distributions were uniformly deposited onto the GO surface and the resulting composites can be used in optoelectronic applications. Ullah et al. reported fast and facile synthesis of Pt/graphene nanocomposite via microwave assisted techniques. They also tested the visible light photo-catalytic activities of Pt/graphene nanocomposite by employing of rhodamine B (Rh.B) and methylene blue (MB) as standard model dyes and in hydrogen evolution processes [21,22]. Chandra et al. studied on the preparation of Mn_2O_3 decorated graphene nano-sheet, via a one-step sonochemical route, as an advanced material for the photocatalytic degradation of organic dyes [23]. Preparation and characterization of different types of metal or metal oxide nanoparticles decorated graphene sheets and investigation of such materials in photo-catalytic elimination processes of organic dyes have been studied [24,25].

In this work, decoration of graphene nano sheets with platinum (Pt) and palladium (Pd) nanoparticles via chemical oxidation-reduction route and the characterization of structural and morphological features of resulted graphene-metal nanocomposites were studied. Furthermore, the antioxidant activity of nanocomposite samples were determined by using of three different spectroscopic assays and finally the catalytic activity of samples was quantified for the photo-degradation processes of two organic dyes.

2. Experimental study

2.1. Materials

Ammonia solution (NH_3 %25), sodium borohydride ($NaBH_4$), platinum (II) chloride ($PtCl_2$), palladium (II) chloride ($PdCl_2$), potassium persulfate ($K_2S_2O_8$), ethanol and methanol were purchased from Merck and Sigma–Aldrich. All the chemicals employed in the study were analytical grade and used as-received without a purification. Reactive agents used in the antioxidant activity analysis were 2,2-azinobis (3-ethyl-benzothiazoline-6-sulfonic acid) (ABTS), bis(neocuproine:2,9-dimethyl-1,10-phenanthroline) copper(II) and 2,2-diphenyl-1-picrylhydrazyl (DPPH).

Commercial grade graphite, thermally expanded powder TIMREX® BNB909, kindly provided by IMERYS Carbon & Graphite (Switzerland) was used as starting material to prepare graphene nano sheets. The density, surface area, average particle size (d_{90}) and the oil adsorption number (OAN) values of expended graphite (EG) particles were reported as 2.24 g cm^{-3}, 28 m^2 g^{-1}, 85.2 μm and 150 ml 100 mg^{-1}, respectively by the producer.

2.2. Decoration of graphene nano-sheets with Pd and Pt nanoparticles

In the first step, EG flakes were oxidized according to the well-known modified Hummers [26] method to prepare graphite oxide (EGO) by using of sulfuric acid (H_2SO_4, fuming), hydrogen peroxide (H_2O_2), potassium permanganate ($KMnO_4$) and sodium nitrate ($NaNO_3$). Then, the EGO was reduced by using of hydrazine monohydrate as reducing agent. The resulted sample was in fact the chemically synthesized graphene nano-sheets but denoted as the reduced expanded graphite oxide (REGO). The detailed explanation for the oxidation and reduction processes and the structural characterization of EG, EGO and REGO were previously reported [27].

Graphene nano-sheets (or REGO sheets) were then dispersed into an ethylene glycol solution and sonicated for 1 h. Subsequently, proper amount of metal (Pd or Pt) chloride solution (5 mg/mL) was added to the mixture and sonicated for 2 h. The pH value of the mixture was adjusted to 11 by using of NaOH solution and the mixture was vigorously stirred under argon atmosphere at 140 °C for 5 h. Then, $NaBH_4$ solution was drop-wisely added into the mixture by continuously stirring the medium for 1 h, under the ambient conditions. The solid fraction of the mixture, graphene-metal nanocomposite, was finally centrifuged, washed with deionized water several times and dried in a vacuum oven at 45 °C for 24 h.

2.3. Structural and morphological characterization of graphene-metal nanocomposites

Microstructural and morphological properties of samples were characterized with X-Ray diffraction (XRD), Fourier-Transform infrared spectroscopy (FTIR), scanning electron microscopy (SEM) and transmission electron microscopy (TEM) methods.

The XRD analysis of samples were performed with a Rigaku-Smart Lab. wide angle X-ray diffractometer with Cu-K_α, running at 40 kV and 40 mA, at room temperature in the range of 20°–70° with the step of 2° per minute. FTIR spectra were recorded in transmission mode with a Bruker-Alpha infrared spectrometer by using an attenuated total reflectance (ATR) apparatus, in the wavenumber range of 400–4000 cm^{-1} with the resolution of 2 cm^{-1}. The morphological features of graphene-metal nanocomposites were examined with a FEI Quanta FEG 450 field emission scanning electron microscope (FESEM) and FEI Tecnai G2 Sphera transmission electron microscope (TEM) after a proper sample preparation steps for the both analysis.

2.4. Determination of antioxidant activity of nanocomposites

Antioxidant activities (AOA) of graphene-metal nanocomposites were determined with the spectroscopic measurements according to three different and the most widely used protocols by employing of specified reactive oxidizing species; 2,2-azinobis(3-ethyl-benzothiazoline-6-sulfonic acid) (ABTS), bis(neocuproine:2,9-dimethyl-1,10-phenanthroline)copper(II) in the cupric reducing antioxidant capacity (CUPRAC) method and 2,2-diphenyl-1-picrylhydrazyl (DPPH). Information on the assays and the

experimental details about the procedures can also be found elsewhere.

The ABTS method is based on the ability of hydrogen or electron-donating antioxidants to decolorize the performed radical monocation of ABTS generated with oxidation of ABTS with potassium persulfate. Seven milimolar (mM) of ABTS solution was added to 2.45 mM $K_2S_2O_8$ solution to produce $ABTS^{\bullet+}$ and the solution was stored in the dark at 25 °C for 12 h. The prepared solution was diluted with ethanol to get an absorbance of 0.700 ± 0.025 at 734 nm. $ABTS^{\bullet+}$ solution (160 μL) was then added into sample solutions having the concentrations of 10, 25, 50, 100 and 200 μg/ml. After 30 min, the inhibition (%) was determined by using the absorbance values measured at 734 nm for each concentration relative to a blank (ethanol). The following equation was used to calculate the scavenging capability of $ABTS^{\bullet+}$ [28].

In the DPPH analysis, 160 μL of 0.1 mM DPPH solution in methanol was added to 40 μL of sample solutions prepared in methanol with the given concentrations. After 30 min, the inhibition (%) was determined by using the absorbance values measured at 517 nm for each concentration relative to a blank. The DPPH free radical scavenging potential was calculated by using the following equation [29].

In the CUPRAC method [30], aliquots of 61 mL of 1.0×10^{-2} M copper (II) chloride, 61 μL of NH_4OAc buffer (1 M, pH 7.0), and 61 μL of 7.5×10^{-3} M neocuproine solution were mixed, then x μL of sample solution (2.5, 6.25, 12.5, and 25 μL) and (67 − x) μL of distilled water were added into the solution to make the final volume of 250 μL. Absorbance values were measured at 450 nm at room temperature after an hour. The results were used to calculate $A_{0.50}$ values. Ethanol was used as control.

2.5. Determination of catalytic activity of nanocomposites for organic dye degradation

Catalytic activity of graphene-metal nanocomposites for the degradation of dye molecules were studied with batch mixing experiments. Chemical structures of dye molecules used in the study are given in Fig. 1.

25 mg of solid sample (REGO and graphene-metal nanocomposites) was added into 50 mL of 100 ppm dye solution in a 100 mL glass beaker The mixture was first stirred in dark condition for 10 min to allow the dye molecules adsorbed physically onto graphene sheets. Then the mixture was kept stirring at ambient conditions under the sun light. 1 ml of sample was taken from the mixture and the dye solution was immediately separated from the solid catalyst by centrifuge at time intervals of 10 min. The supernatant was used in the UV analysis to follow the photocatalytic degradation reaction. UV–Vis spectrophotometric measurements were carried out using a Hitachi U-2900 UV–Visible spectrophotometer having in the scan range 250–400 nm^{-1} and a spectral resolution of 1 nm.

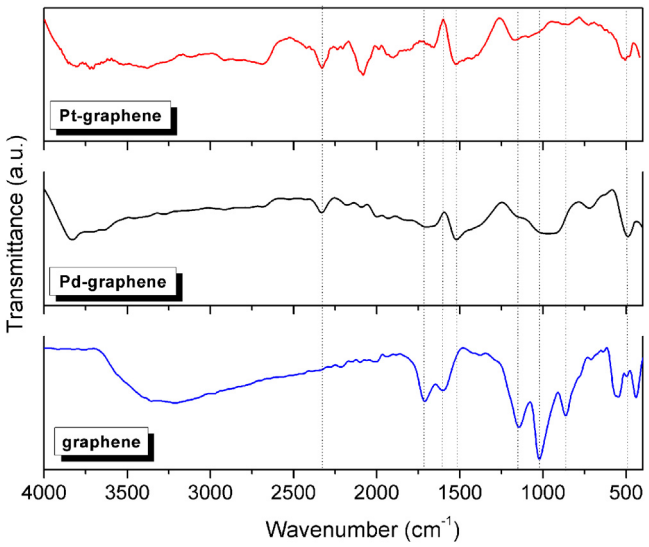

Fig. 2. FTIR spectrum of graphene and graphene-metal nanocomposites.

3. Results and discussion

3.1. Structural characterization of graphene-metal nanocomposites

Fig. 2 shows the FTIR spectrum of graphene (also denoted as REGO) sheets and nanocomposites.

FTIR spectra of graphene sheets showed the following characteristic bands; stretching vibration of carbonyl (C=O) bonds at the wavenumber of 1710 cm^{-1}, ring vibrations of carbon–carbon double bonds (C=C) at 1602 cm^{-1}, stretching vibration of carbon-hydroxyl (C–OH) bonds at 1160 cm^{-1} and stretching of epoxide groups (C–O) at 1056 cm^{-1} [31]. These peaks can be attributed to the fact that little amount of oxygen species originated from the carbonyl, carboxyl and epoxide groups were still present onto the graphene sheets possibly due to the uncompleted chemical reduction of graphene oxide. FT-IR spectrum of Pd-graphene and Pt-graphene nanocomposites also exhibited several functional peaks corresponding to hydroxyl (O–H) groups at about 3800 cm^{-1}, C=C bending at 1530 cm^{-1} and C–O stretching at 980 cm^{-1}. It could be clearly seen that the intensities of such peaks were smaller than those observed in the FTIR spectra of graphene due to the possible interactions between metals sites with the hydroxyl and carboxyl groups. A distinctive peak observed at wavenumber of 500 cm^{-1} signified the formation of metal-oxygen bonding for the graphene-metal nanocomposites. It is well-known

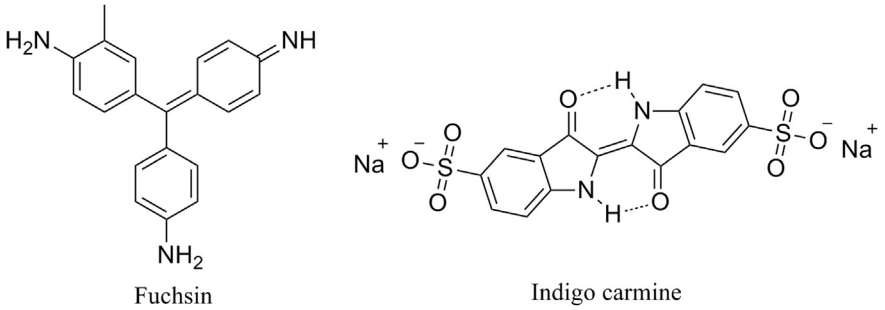

Fig. 1. Chemical structures of organic dyes used in the study.

that the metal-graphene bonding occurs through van der Waals force, H-bonding and other physical or chemical interactions. Metal atoms may possibly interact with the remaining hydroxyl and carboxyl groups onto the graphene sheets to form C–O–Me or O=C–O–Me bonds via dehydration reactions [32].

Fig. 3 shows the XRD patterns of the graphene-metal nanocomposites between the diffraction angle range of 20°–70°. Three distinctive diffraction peaks at 39.8°, 46.5° and 67.8° which correspond to the (111), (200) and (220) crystal planes of face-centered-cubic (*fcc*) phase of bulk metals, Pt and Pd, can be clearly seen in the XRD patterns of the nanocomposites. Two small peaks (denoted with the +) observed in the XRD pattern of Pd-graphene sample at the diffraction angles about 29° (002) and 43° (110) might correspond to the formation of PdO (JCPDS Card No of 41–1107) [33]. The average crystallite sizes (D) of the metal particles could be determined with the well-known Debye-Scherrer's equation defined as;

$$D = \frac{K\lambda}{\beta \mathrm{Cos}\theta} \quad (1)$$

where D is the average size of the crystalline domains, K is a dimensionless shape factor (typical value of about 0.9), λ is the X-ray wavelength (0.154 nm), β is the full width at half-maximum (FWHM) of the diffraction peak in radian, and θ is the Bragg angle. The average crystallite size of Pt and Pd nanoparticles were determined to be 7.5 ± 0.8 and 8.2 ± 1.0 nm, respectively. This result implied that the average crystallite sizes of noble metal nanoparticles onto graphene sheets were quite similar. These values are somewhat smaller than those previously reported and structurally similar metal-graphene nanocomposites [34]. The XRD analysis of samples obviously confirmed that the platinum and palladium salts were successfully reduced by using of $NaBH_4$ onto graphene sheets and formed metal nanoparticles.

The relatively small peak, marked with the star (*) and seen about 2θ of 25°, corresponds to the typical (002) planes of graphene layers. It is well-known that the graphite stacks, consisting of thousands of graphene layers, showed a characteristic very intense and sharp peak in this region. Oxidation of graphene shifts this peak to lower diffraction angles about 2θ = 10–12° due to the intercalation of chemical species through inter gallery spaces and expansion of graphene layers and the formation of graphene oxide (GO). An effective chemical reduction removes the organic species between graphene layers and generally yields disordered (or exfoliated) structure characterized with no peak in the XRD pattern. The broad and relatively small peak seen at 2θ = 10–12° in the XRD patterns of graphene-metal nanocomposites can be attributed to the fact that the oxygen species did not completely removed from the graphene sheets, as previously discussed [27].

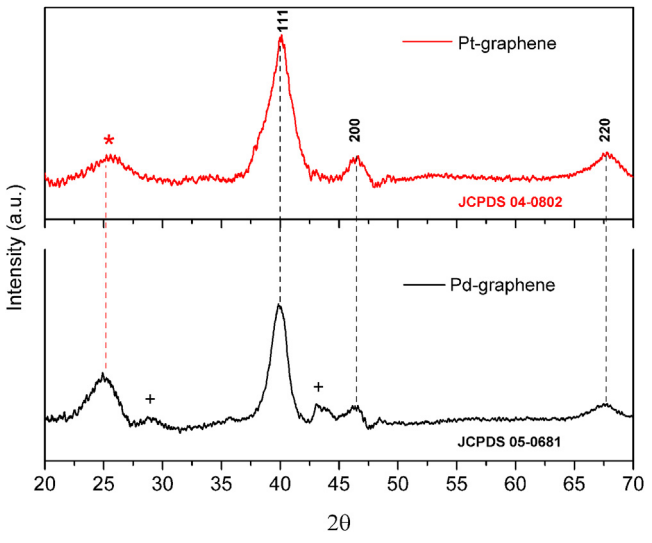

Fig. 3. XRD patterns of graphene-metal nanocomposites.

Fig. 4(a–f) illustrates the SEM and TEM images of graphene and graphene-metal nanocomposites to understand the morphological features of samples.

Representative SEM and TEM images of reduced graphene oxide sheets, given in Fig. 4(a) and (b), display wrinkled and transparent graphene layers having an average lateral size in the range of 8–12 μm. As seen in these images, surface of graphene sheets is quite smooth. Fig. 4(c and f), exemplify the SEM and TEM micrographs of Pt-graphene and Pd-graphene nanocomposites, respectively. It is clearly seen in these images that the both Pt and Pd nanoparticles were successfully formed and homogenously dispersed onto graphene sheets. Especially in the SEM images of samples, morphological features of metal-graphene nanocomposites can be evidently noticed and compared. It is obvious that the average size of Pd nanoparticles were slightly smaller than that of Pt nanoparticles and Pd nanoparticles also showed more uniform distribution. In The SEM and TEM images of Pt-graphene nanocomposite, it was also seen that the Pt dispersed as relatively bigger domains and formed nano-size unshapen agglomerations compared to Pd nanoparticles.

3.2. Antioxidant activity of graphene-metal nanocomposites

The ABTS and DPPH free radical scavenging activity values of graphene-metal nanocomposites are given in Fig. 5.

The radical scavenging activity of graphene-metal nanocomposites can be expressed with the IC_{50} values. The IC_{50} values of Pt-graphene and Pd-graphene nanocomposites were found to be 46.1 and 90.2 μg/mL, respectively based on the ABTS method. On the other hand, the IC_{50} values of Pt-graphene and Pd-graphene nanocomposites were determined as 80.2 and 143.7 μg/mL, respectively according to the DPPH method. The CUPRAC method yielded the $A_{0.5}$ value of 42.7 μg/mL for the Pt-graphene and 62.5 μg/mL for the Pd-graphene nanocomposite. One can notice that the DPPH method yielded higher IC_{50} values than the ABTS method for both graphene-metal nanocomposites. Furthermore, the IC_{50} values of Pt-graphene nanocomposite were lower than those of Pd-graphene counterpart. It was possibly due to the fact that the amount of metal or metal/carbon atomic ratio in the Pt-graphene sample was higher than that of in the Pd-graphene counterpart. This was also proved with the EDS analysis as a semi-quantitative method but not reported here.

These results indicate that the graphene nano-sheets decorated with Pt and Pd nanoparticles show extremely high antioxidant activity compared to reduced graphene oxide (rGO) or noble metal nanoparticles synthesized by using of green chemicals as reducing agents. It should be noted that the IC_{50} values of Pt-graphene and Pd-graphene nanocomposite are approximately 20-fold and 11-fold lower than that of rGO reported by Suresh et al. (IC_{50} = 1590 μg/ml) based on the DPPH method [35]. They also reported an IC_{50} value of 1337 μg/ml for an rGO synthesized by using of another green reductant, clove extract [36]. Mani et al. studied on the antioxidant properties of the biosynthesized silver nanoparticles by using the DPPH assay and they found that the IC_{50} value of Ag nanoparticles having the particle size of 40–60 nm was 183.24 + 0.93 μg/mL [37]. Saritha and Saraswathi determined the DPPH-based free radical scavenging activity of Au nanoparticles synthesized via a green-reduction method as 0.25 mg/mL (250 μg/mL) [38]. On the other hand, the IC_{50} values of graphene-metal nanocomposites were

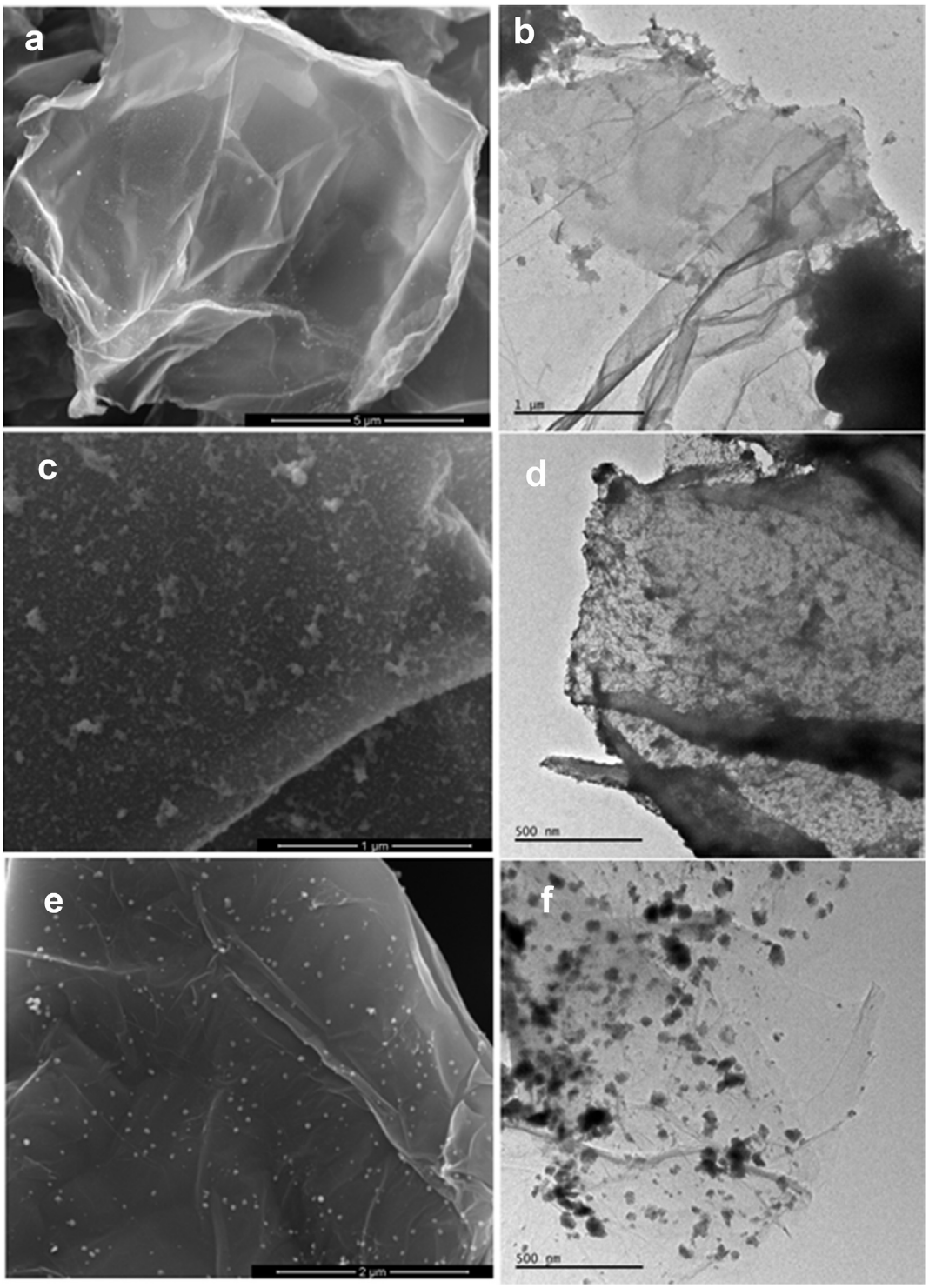

Fig. 4. SEM micrographs of a) graphene, c) Pt-graphene and e) Pd-graphene and TEM images of b) graphene, d) Pt-graphene and f) Pd-graphene nanocomposites.

found to be somewhat higher than those of various types of noble metal nanoparticles such as Au and Ag etc. For example, Parveen et al. reported that the IC_{50} values of silver nanoparticles (AgNPs) synthesized with a microwave-assisted green method was 5.71 µg/mL [39]. It can be expected that the free radical scavenging activity values of graphene-metal nanocomposites could be lower than those of plain and nano-size metal particles because the nanocomposites consist of much lower (about more than a ten-fold) amount of active metal sites than the nano-crystalline metal powders.

3.3. Catalytic activity of graphene-metal nanocomposites for organic dye degradation

Time dependent UV spectrum of dyes, indicating the photodegradation reactions onto graphene-metal nanoparticles, are

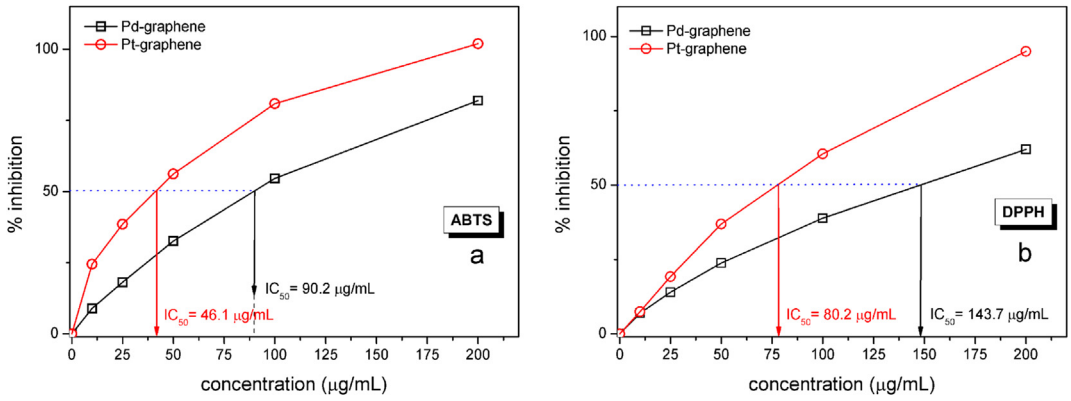

Fig. 5. Free radical scavenging activity of graphene-metal nanocomposites according to the (a) ABTS and (b) DPPH assays.

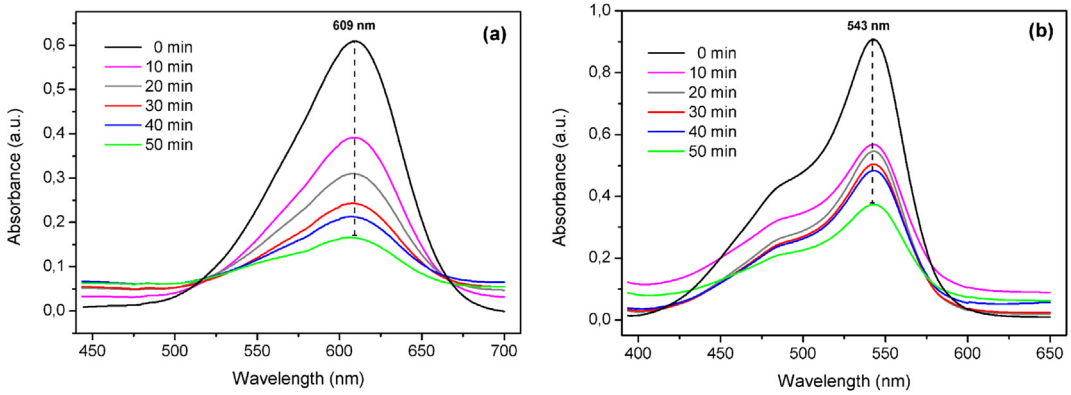

Fig. 6. Time dependent UV peaks of (a) indigo carmine and (b) fuchsin onto Pt-graphene nanocomposite.

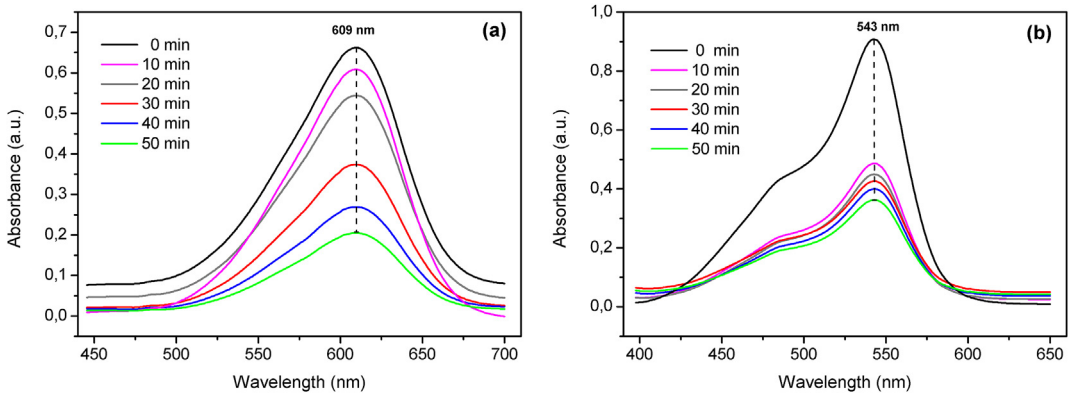

Fig. 7. Time dependent UV peaks of (a) indigo carmine and (b) fuchsin onto Pd-graphene nanocomposite.

given in Fig. 6 and Fig. 7 for the Pt-graphene and Pd-graphene nanocomposites, respectively.

Variation in the characteristic peak intensity can be originated from the initial physical adsorption of dye molecules onto graphene sheets and further chemical elimination of dyes due to the photo catalytic reactions induced by the active metal sites onto graphene sheets. In this study, first 10 min was considered as the physical adsorption step. As seen in the Figs. 7 and 8, time-dependent behaviors of dyes were significantly different. It was observed that the characteristic absorbance of indigo carmine at the wavelength of 609 nm gradually decreased with the increasing of time for both graphene-metal nanocomposites. On the other hand, the characteristic peak of fuchsin rapidly reduced for the first 10 min then the intensity of peak slowly decreased with time.

It can also be accepted that these trends reflect the rate of reaction. In literature, it has been generally accepted that the photocatalytic degradation reactions of dye molecules can be expressed with the first-order or pseudo first-order kinetic equations expressed as;

$$-\frac{dC}{dt} = k_{app}C \tag{2}$$

where C is the concentration of sample (C=C_0 at $t = 0$, C_0 is the

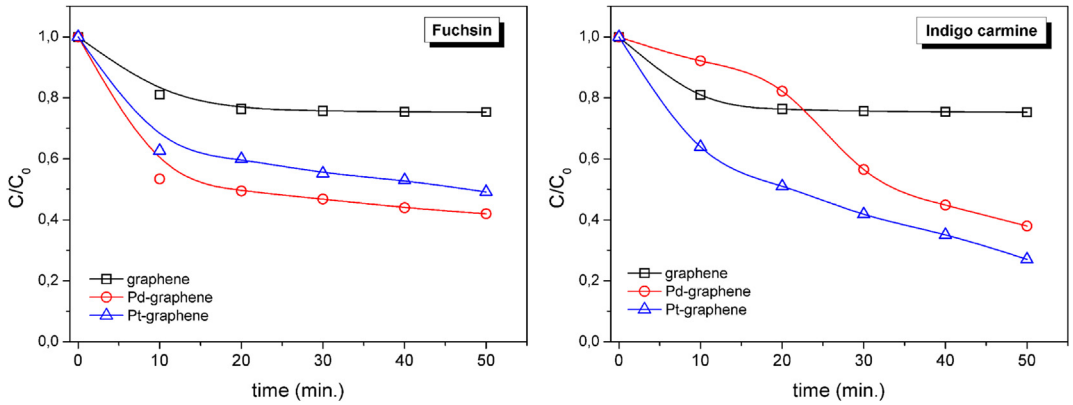

Fig. 8. Kinetic curves of elimination of Fuchsin and Indigo carmine dyes onto graphene, Pd-graphene and Pt-graphene nanocomposites.

initial concentration of dye solution), k_{app} is the apparent reaction rate constant and t is time. The C/C_0 versus time curves given in Fig. 8, can be used to follow and compare the reactions.

As seen in Fig. 8, the neat graphene adsorbed some part of dyes within 10 min then the concentration of dyes in the supernatant showed almost no changes. It can be concluded that the catalytic activity of Pd-graphene was slightly higher than that of Pt-graphene for the degradation of fuchsin under light irradiation. On the other hand, Pt-graphene nanocomposite exhibited higher activity than the Pd-graphene counterpart for the degradation of indigo carmine. Fig. 8 also implies that the degradation rate of indigo carmine possibly higher than that of fuchsin for the given conditions by considering the slope of C/C_0 curves. The C/C_0 curves of both nanocomposites decreased slowly with time between 10 and 50 min under the light irradiation conditions for fuchsin.

Photocatalytic effect of noble metal decorated graphene nanocomposites for the photocatalytic degradation of organic dye molecules and possible reaction mechanism is illustrated in Fig. 9.

Reaction mechanism is basically based on the electrochemical interactions between conducting graphene and metal nanoparticles as a result of the photonic excitations of metal nanoparticles and the reactions between the radical species and organic molecules as previously explained, in detail [40–42]. As shown in the figure, visible light first excites the metal surface plasmon and produces energetic electrons at the surfaces of nanoparticles. Then those electrons quickly transports to the extended π-conjugation of graphene via the interface between the graphene and metal nanoparticle surfaces and leads to the efficient separation of electron–hole pairs, as. Those electrons react with dissolved oxygen in the reaction medium to produce reactive oxygen species and holes on the metals. Reactive oxygen species then react with water molecules to produce hydroxyl radicals which lead to degradation of organic molecules. Bhunia and Jana concluded that the loading of metal nanoparticles controls the photoexcited electron–hole pairs, and the rest of the rGO surface is used for attachment of organic molecules in their work investigated the photocatalytic activity of rGO-Ag nanocomposites [11]. They also accentuated that an optimum metal loading is an important parameter for balancing of both these requirements. They concluded that the rate of photocatalytic degradation process is slow in the case of both low and high loadings of metal nanoparticles because the relatively low amount of metal cannot produce sufficiently enough reactive oxygen species and the high amount of metal may block the large surface area of graphene sheets and thus the organic molecules cannot be absorb on the graphene surface.

4. Conclusion

In this study, graphene nano-sheets were successfully decorated with the Pt and Pd nanoparticles via chemical reduction method.

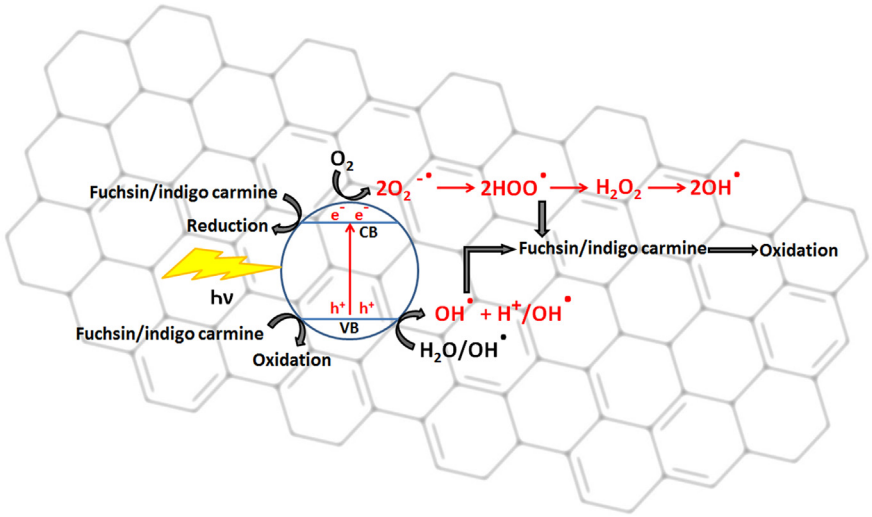

Fig. 9. Schematic illustration of possible photocatalytic degradation mechanism of organic dyes onto graphene-noble metal nanocomposites. (VB: valance band, CB: conduction band).

Based on the XRD, SEM and TEM analysis, the crystallite size of metal nanoparticles were found to be lower than 10 nm and nanoparticles were uniformly dispersed onto graphene sheets. It was also found that the graphene metal nanoparticles exhibited significantly high free radical scavenging activity compared to previously reported results for graphene and metal nanoparticles. Catalytic activities of Pt-graphene and Pd-graphene nanocomposites were quantified for the elimination of fuchsin and indigo carmine dyes. Consequently, it was shown that the graphene-metal nanocomposites can be used as novel type nano-structured catalysts for photocatalytic degradation reactions of organic dyes in aqueous medium.

References

[1] C. Bosch-Navarro, E. Coronado, C. Marti-Gastaldo, Controllable coverage of chemically modified graphene sheets with gold nanoparticles by thermal treatment of graphite oxide with N,N-dimethylformamide, Carbon 54 (2013) 201–207.

[2] A.K. Geim, K.S. Novoselov, Rise of graphene, Nat. Mater. 6 (2007) 183–191.

[3] H. Kim, A.A. Abdala, C.W. Macosko, Graphene/polymer nanocomposites, Macromolecules 43 (2010) 6515–6530.

[4] L. Pauksch, S. Hartmann, M. Rohnke, G. Szalay, V. Alt, R. Schnettler, K.S. Lips, Biocompatibility of silver nanoparticles and silver ions in primary human mesenchymal stem cells and osteoblasts, Acta Biomater. 10 (2014) 439–449.

[5] H. Quan, Y. Shao, C. Houa, Q. Zhang, H. Wang, Y. Li, Room-temperature synthesis of 3-dimensional Ag-graphene hybrid hydrogel with promising electrochemical properties, Mater. Sci. Eng. B 178 (2013) 769–774.

[6] J. Lu, I. Do, L.T. Drzal, R.M. Worden, I. Lee, Nanometal-decorated exfoliated graphite nanoplatelet based glucose biosensors with high sensitivity and fast response, ACS Nano 2 (2008) 1825–1832.

[7] Z. Xiong, L.L. Zhang, J. Ma, X.S. Zhao, Photocatalytic degradation of dyes over graphene–gold nanocomposites under visible light irradiation, Chem. Commun. 46 (2010) 6099–6101.

[8] W. Yi, J. Liu, H.B. Chen, Y. Gao, H.M. Li, Copper/nickel nanoparticle decorated carbon nanotubes for nonenzymatic glucose biosensor, J. Solid State Electrochem. 19 (2015) 1511–1521.

[9] Y. Tepeli, U. Anik, Comparison of performances of bioanodes modified with graphene oxide and graphene–platinum hybrid nanoparticles, Electrochem. Commun. 57 (2015) 31–34.

[10] J. Shen, M. Shi, N. Li, B. Yan, H. Ma, Y. Hu, M. Ye, Facile synthesis and application of Ag-chemically converted graphene nanocomposite, Nano Res. 3 (2010) 339–349.

[11] S.K. Bhunia, N.R. Jana, Reduced graphene oxide-silver nanoparticle composite as visible light photocatalyst for degradation of colorless endocrine disruptors, ACS Appl. Mater. Interfaces 6 (2014) 20085–20092.

[12] A. Roucoux, J. Schulz, H. Patin, Reduced transition metal colloids: a novel family of reusable catalysts? Chem. Rev. 102 (2002) 3757–3778.

[13] K.B. Narayanan, H.H. Park, Pleiotropic functions of antioxidant nanoparticles for longevity and medicine, Adv. Colloid Interface Sci. 201–202 (2013) 30–42.

[14] Y. Yoshihisa, A. Honda, Q.-L. Zhao, T. Makino, R. Abe, K. Matsui, H. Shimizu, Y. Miyamoto, T. Kondo, T. Shimizu, Protective effects of platinum nanoparticles against UV-light-induced epidermal inflammation, Exp. Dermatol. 19 (2010) 1000–1006.

[15] M. Kajita, K. Hikosaka, M. Iitsuka, A. Kanayama, N. Toshima, Y. Miyamoto, Platinum nanoparticle is a useful scavenger of superoxide anion and hydrogen peroxide, Free Radic. Res. 41 (2007) 615–626.

[16] Y. Yoshihisa, Q.L. Zhao, M.A. Hassan, Z.L. Wei, M. Furuichi, Y. Miyamoto, T. Kondo, T. Shimizu, SOD/catalase mimetic platinum nanoparticles inhibit heat-induced apoptosis in human lymphoma U937 and HH cells, Free Radic. Res. 45 (2011) 326–335.

[17] A. Watanabe, M. Kajita, J. Kim, A. Kanayama, K. Takahashi, T. Mashino, Y. Miyamoto, In vitro free radical scavenging activity of platinum nanoparticles, Nanotechnology 20 (2009) 455105.

[18] I. Do, L.T. Drzal, Room temperature ionic liquids for size control of noble metal nanoparticles on carbon supports, Carbon 75 (2014) 43–55.

[19] E. Garridoa, C. Aymonier, L. Roibanc, O. Ersen, C. Labrugèrea, P. Gaillard, M. Lamirand-Majimel, Noble metals supported on carbon nanotubes using supercritical fluids for the preparation of composite materials: a look at the interface, J. Supercrit. Fluids 101 (2015) 110–116.

[20] C. Zheng, W.Z. Chen, Y.Y. Huang, X.Q. Xiao, X.Y. Ye, Graphene oxide-noble metal (Au, Pt, and Pd) nanoparticle composites as optical limiters, RSC Adv. 4 (2014) 39697–39703.

[21] K. Ullah, S. Ye, L. Zhu, Z.-D. Meng, S. Sarkar, W.-C. Oh, Microwave assisted synthesis of a noble metal-graphene hybrid photocatalyst for high efficient decomposition of organic dyes under visible light, Mater. Sci. Eng. B 180 (2014) 20–26.

[22] K. Ullah, S. Ye, L. Zhu, S.B. Jo, W.K. Jang, K.-Y. Cho, W.-C. Oh, Noble metal doped graphene nanocomposites and its study of photocatalytic hydrogen evolution, Solid State Sci. 31 (2014) 91–98.

[23] S. Chandra, P. Das, S. Bag, R. Bhar, P. Pramanik, Mn_2O_3 decorated graphene nanosheet: an advanced material for the photocatalytic degradation of organic dyes, Mater. Sci. Eng. B 177 (2012) 855–861.

[24] Z. Gao, J. Liu, F. Xu, D. Wu, Z. Wu, K. Jiang, One-pot synthesis of graphene-cuprous oxide composite with enhanced photocatalytic activity, Solid State Sci. 14 (2012) 276–280.

[25] E.S. Agorku, M.A. Mamo, B.B. Mamba, A.C. Pandey, A.K. Mishra, Palladium-decorated zinc sulfide/reduced graphene oxide nanocomposites for enhanced visible light-driven photodegradation of indigo carmine, Mater. Sci. semiconduc. Process 33 (2015) 119–126.

[26] W.S. Hummers, R.E. Offeman, Preparation of graphitic oxide, Am. Chem. Soc. 80 (1958), 1339–1339.

[27] Z. Durmus, A. Durmus, H. Kavas, Synthesis and characterization of structural and magnetic properties of graphene/hard ferrite nanocomposites as microwave-absorbing material, J. Mater. Sci. 50 (2015) 1201–1213.

[28] R. Re, N. Pellegrini, A. Proteggente, A. Pannala, M. Yang, C.R. Evans, Antioxidant activity applying an improved ABTS radical cation decolorization assay, Free Radic. Bio. Med. 26 (1999) 1231–1237.

[29] W. Brand-Williams, M.E. Cuvelier, C. Berset, Use of a free radica method to evaluate antioxidant activity, Food Sci. Technol. 28 (1995) 25–30.

[30] R. Apak, K. Guclu, M. Ozyurek, S.E. Karademir, Novel total antioxidant capacity index for dietary polyphenols and vitamins C and E, using their cupric ion reducing capability in the presence of neocuproine: CUPRAC method, J. Agric. Food Chem. 52 (2004) 7970–7981.

[31] Y. Yu, Y. Li, Y. Pan, C.-J. Liu, Fabrication of palladium/graphene oxide composite by plasma reduction at room temperature, Nanoscale Res. Lett. 7 (2012) 234.

[32] F. Chekin, Sol–gel synthesis of palladium nanoparticles supported on reduced graphene oxide: an active electrocatalyst for hydrogen evolution reaction, Bull. Mater. Sci. 38 (2015) 887–893.

[33] A. Ohtaka, T. Yamaguchi, T. Teratani, O. Shimomura, R. Nomura, Linear polystyrene-stabilized PdO nanoparticle-catalyzed Mizoroki-Heck reactions in water, Molecules 16 (2011) 9067–9076.

[34] J.-X. Fenga, Q.-L. Zhang, A.-J. Wang, J. Wei, J.-R. Chen, J.-J. Feng, Caffeine-assisted facile synthesis of platinum@palladium core-shell nanoparticles supported on reduced graphene oxide with enhanced electrocatalytic activity for methanol oxidation, Electrochim. Acta 142 (2014) 343–350.

[35] D. Suresh, P.C. Nethravathi, Udayabhanu, H. Nagabhushana, S.C. Sharma, Spinach assisted green reduction of graphene oxide and its antioxidant and dye absorption properties, Ceram. Int. 41 (2015) 4810–4813.

[36] D. Suresh, Udayabhanu, H. Nagabhushana, S.C. Sharma, Clove extract mediated facile green reduction of graphene oxide, its dye elimination and antioxidant properties, Mater. Lett. 142 (2015) 4–6.

[37] A. Mani, S. Lakshmi, V. Gopal, Bio-mimetic synthesis of silver nanoparticles and elavulation of its free radical scavenging activity, Inter. J. bio. Pharm. Res. 3 (2012) 631–633.

[38] K. Saritha, U. Saraswathi, Antioxidant activity of gold nanoparticles synthesized using *Lemna minor*, World J. Pharm. Sci. 2 (2014) 1545–1551.

[39] M. Parveen, F. Ahmad, A.M. Malla, S. Azaz, Microwave-assisted green synthesis of silver nanoparticles from *Fraxinus excelsior* leaf extract and its antioxidant assay, Appl. Nanosci. (2015), http://dx.doi.org/10.1007/s13204-015-0433-7.

[40] I.V. Lightcap, T.H. Kosel, P.V. Kamat, Anchoring semiconductor and metal nanoparticles on a two-dimensional catalyst mat. storing and shuttling electrons with reduced graphene oxide, Nano Lett. 10 (2010) 577–583.

[41] Z. Mou, Y. Wu, J. Sun, P. Yang, Y. Du, C. Lu, TiO_2 nanoparticles-functionalized N-doped graphene with superior interfacial contact and enhanced charge separation for photocatalytic hydrogen generation, ACS Appl. Mater. Interfaces 6 (2014) 13798–13806.

[42] X.F. Yang, H.Y. Cui, Y. Li, J.L. Qin, R.X. Zhang, H. Tang, Fabrication of Ag_3PO_4-graphene composites with highly efficient and stable visible light photocatalytic performance, ACS Catal. 3 (2013) 363–369.